Assessment of Urban Heat Island Effects in Awka Metropolis, Anambra State

[1]Ezezue, A.M, [2]Abazuonu, L.C., [3]Enete, I.C. and [4]Odoanyanwu, N.M
[1, 2, 4] Department of Architecture,Nnamdi Azikiwe University, Awka, Anambra State
[3]Department of Geography and Meteorology, Nnamdi Azikiwe University, Awka, Anambra State

Abstract
This paper was aimed at assessing the magnitude of urban heat island in Awka metropolis using satellite derived data and shuttle radar topographic mission (SRTM) covering the study area. The land surface temperature was estimated using the low gain thermal band from Landsat imagery. Solar radiation characteristics were also calculated from the satellite imagery using solar radiation algorithm. The Normalised Difference Vegetation Index (NDVI) was used in determining the reflectance values of various surface types. The result showed that towns within Awka North and parts of Awka South experiences relatively high temperature within the range of 30 to 38^{o}C more than the other towns. Awka city centre exhibited the highest temperature value. It was also observed that areas with high temperature value are relatively covered with artificial surfaces with low vegetal cover.

Keywords: Urban Heat, Surface Temperature, Awka , Solar Radiation, Landsat Imagery.

Introduction

Over the past years, the rate of urban growth has speeded up and extreme stress to the environment has occurred. This is particularly true in major cities and towns such as Lagos, Ibadan among others, where there is increasing influx of people and massive agricultural land is disappearing each year, converted to urban or related uses (Hara, Takeuchi, & Okubo, 2005). Evaluating the magnitude and pattern of this urban growth is an urgent need.Furthermore, because of the lack of appropriate land use planning and the measures for sustainable development, rampant urban growth has been creating severe environmental consequences. There is thus a need to assess the environmental impact of the rapid urban expansion. The warming trends due to urban heat islands are growing all over the world. It is therefore important to study this phenomenon and understand the mechanism for efficient city planning.

Land surface temperatures are most important in global change studies as they are used in the estimation of radiation budget, heat balance and in climatic modelingmostly in the urban areas (Wubet, 2003) quoted by (El-Sayed, 2012). Land surface temperature is a component of urban heat Island effects. Urban Heat Island (UHI) is an identified environmental phenomenon where air and land surface temperatures (LST) of urban areas are higher than those of the surrounding rural areas (Ahmed, Kamruzzaman, Zhu, & Rahman, 2013). As a result, LST and UHI are often used interchangeably in this reaserch work. Land cover changes (e.g., from vegetation to impervious cover such as pavement, roofs, asphalt), again, are the main causes of changing LST because each land cover type possesses unique qualities in terms of energy radiation and absorption (Ahmed, *et al.,* 2013).

Recent studies on the impact of these changing land cover on the LST have been intensified due to the availability of remote sensing databases of an area for different time periods (Ahmed, et al., 2013). The concept of UHI was described by Luke Howard in 1833 and, since then, research on this topic gradually intensified (Howard,

1833). In a broader geographical context, UHI is a metropolitan area, which is significantly warmer than its surrounding rural areas. However, UHI can also exist within a city region—which implies that a portion of urban area is significantly warmer than its surrounding urban areas (Liu & Zhang, 2011). The temperature difference is usually larger at night, in winter, and under weaker wind condition compared to daytime, summer, and stronger wind condition, respectively (Streutker, 2002). However, a different scenario might also exist depending on spatio-temporal context of an analysis. Ohashi and Kida (2002) have shown that under clear skies and light wind conditions, cities are typically warmer than surrounding rural environments by up to 10 °C. Souch and Grimmond (2006) summarized their findings as: the UHI (1) is primarily a nocturnal phenomenon, (2) can occur throughout the year, (3) is dependent on weather conditions such as wind, and (4) generally consists of higher temperatures in the urban core and commercial locations, with lower temperatures in residential and rural sites.

The integration of remote sensing and Geographic Information System (GIS) provides a powerful way to effectively monitor urban environment and human activities. Satellite borne instruments can provide quantitative physical data at high spatial or temporal resolutions and repetitive coverage and capability of measurements of earth surface conditions (Owen *et al.,* 1998). Voogt and Oke (2003) reviewed the use of thermal remote sensing for the study of urban climates with respect to the heat islands and describe the distinction between the atmospheric and the surface UHIs.

Methodologies

Study Area

The study area which comprises of Awka North, Awka South, Dunukofia,Njikokaand Oyi LGAs is located in Anambra State, South Eastern Nigeria. It covers a total area of 1221.04 km2 with an estimate population of 3,069,164. It extends between Longitude 6˚46'30" E and 7˚7'30" E and Latitude 6˚6'0" N and 6˚27'0" N. The urban, semi-urban and rural towns that make up the study area include: Awka (State Capital), Mbaukwu, Amawbia, Nise, Umuawulu, Achalla, Mgbakwu, Ugbene, Ebenebe, Awba-Ofemili, Amanasa, Isu-Aniocha, Amanuke, Ugbenu, Urum, Ukpo, Umudioka, Ifitedunu, Ukwulu, Umunnachi, Nawgu, Abagana, Nimo, Enugwu-Agidi, Enugwu-Ukwu, Nawfia, Abba, Okpuno, Ezinato, Nibo, Isiagu, Nkwelle, Ogbunike, Nsugbe, Onitsha, Umunnya, Awkuzu, etc (Fig 1). It has a relief which is basically flat lowland with an altitude below 300m (Fig 3). The area is characterised by two main climatic seasons; dry and rainy seasons. The dry season which starts from October to March is accompanied by a dust laden wind from the Sahara desert, known as Harmattan, which is brought by the North Eastern Trade wind from the Sahara desert, while the rainy season which starts from April to September is brought by the South Western trade wind from the Atlantic ocean. The study communities lie within the humid tropical rain forest belt of Southeastern Nigeria. They belong to the Guinea Savanna vegetation type with Localized clustered growth of deep-rooted tall tree (6 meters or more). They also have under growth of tall grasses mostly elephant grass; Awolowo weed and climber trees with durable roots are common.

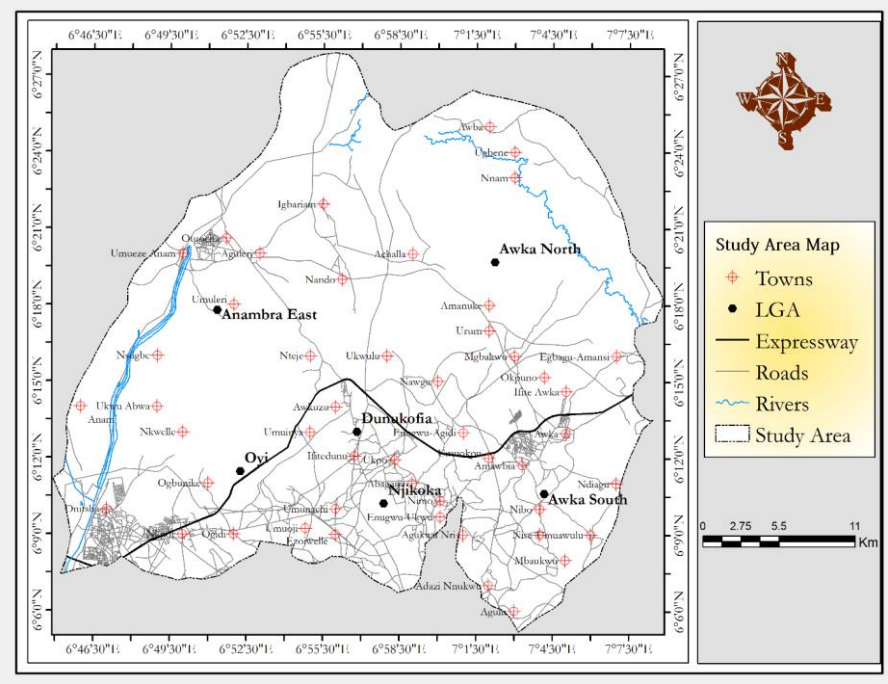


Fig 1: Study Area

Data

The data used for this study include the following; the Administrative Map of Anambra Local Government Areas, Landsat8 OLI/TIR satellite imagery (path189/ row 56) for the dry season period (December, 2016) and Shuttle Radar Topographic Mission (SRTM) covering the study area were acquired from OSGOF and United State Geological Survey (USGS) respectively.

Land Surface Temperature

Asmat, Mansor, & Hong (2003) and Ahmed, Kamruzzaman, Zhu, & Rahman (2013), in mapping of the Urban Heat Island using the rule based classification estimated the surface temperature using the low gain thermal band from Landsat.

To calculate BT which means at brightness temperature, the digital number of the thermal bands were first converted to radiance using the formula (equation 1):

$L_A = M_L Q_{cal} + A_L$ (1) Where L_A = TOA spectral radiance

M_L = Band specific multiplicative rescaling factor from the metadata (Radiance_Multi_Band_x, where x is the band number)

A_L = Band specific additive rescaling factor from the metadata (Radiance_ADD_BAND_x,where x is the band number)
Q_{cal}= Quantized and calibrated standard product pixel values (DN)
From Landsat 8 metadata

M_L = Radiance multiplicative band for bands 10 and 11 = 0.00033420 and 0.00033420
A_L Radiance Add_bandfor bands 10 and 11 = 0.10000 and 0.10000

Q_c = Band 10 or Band 11 Digital number = 0.0003342 + Band 10/ Band 11 + 0.1
To calculate the Brightness Temperature BT

The equation used was: $T = \frac{K_2}{\ln(\frac{K_1}{L_A} + 1)(2)}$

Where:
T = at satellite brightness temperature (k)
L_A = TOA spectral radiance

K_1 = Band specific thermal conversion constant from the metadata (K_1 = constant Band x, where x is the Band number 10 or 11

K_2 = Band Specific thermal conversion constant from the metadata (K_2 =constant Band x, where x is the Band number 10 or 11)

From the metadata, the K_1 and K_2 for bands 10 and 11 are used for the analysis by calculating each of them separately and then combining them so as to get the average using cell statistics under the spatial analyst tool box. The result gotten will be in kelvin but was converted to Celsius by subtracting 272.15 from the equation.
For Band 10, the equation was given as:

$$\frac{1321.08}{\ln(\frac{774.89}{L_A \text{ Band } 10} + 1)} - 272.15 \quad (3)$$

For Band 11, the equation is given as:

$$\frac{1201.14}{\ln(\frac{480.89}{L_A \text{ Band } 11} + 1)} - 272.15 \quad (4)$$

Solar Radiation Algorithm
According to the surface energy budget equation, there is a close relationship between the surface net radiation, land surface albedo, downward shortwave radiation, downward long-wave radiation and land surface emissivity (Tao, et al., 2013) quoted in (Enjun, Xiangzheng, Zhang, & Liu, 2014).

"With landscape scales, topography is a major factor that determines the spatial variability of insolation. Variation in elevation, orientation (slope and aspect), and shadows cast by topographic features all affect the amount of insolation received at different locations. This variability also changes with time of day and time of year and in turn contributes to variability of microclimate including factors such as air and soil temperature regimes, evapotranspiration, snow melt patterns, soil moisture, and light available for photosynthesis"(ESRI, 2014).

The solar radiation analysis tools calculate insolation across a landscape or for specific locations, based on methods from the hemispherical viewshed algorithm developed by Rich et al. (Rich et al. 1994) and further developed by Fu and Rich (2000, 2002).
The total amount of radiation calculated for a particular location or area is given as global radiation. The calculation of direct, diffuse, and global insolation are repeated for each feature location or every location on the topographic surface, producing insolation maps for an entire geographic area.

Solar radiation equations

Global radiation calculation

Global radiation ($Global_{tot}$) is calculated as the sum of direct (Dir_{tot}) and diffuse (Dif_{tot}) radiation of all sun map and sky map sectors, respectively.

$Global_{tot} = Dir_{tot} + Dif_{tot}$ (5)

Direct solar radiation

Total direct insolation (Dir_{tot}) for a given location is the sum of the direct insolation ($Dir_{\theta,\alpha}$) from all sun map sectors:

$Dir_{tot} = \Sigma\ Dir_{\theta,\alpha}$ (6)

The direct insolation from the sun map sector ($Dir_{\theta,\alpha}$) with a centroid at zenith angle (θ) and azimuth angle (α) is calculated using the following equation:

$Dir_{\theta,\alpha} = S_{Const} * \beta^{m(\theta)} * SunDur_{\theta,\alpha} * SunGap_{\theta,\alpha} * \cos(AngIn_{\theta,\alpha})$ (7)

- where:
  - S_{Const} — The solar flux outside the atmosphere at the mean earth-sun distance, known as solar constant. The solar constant used in the analysis is 1367 W/m^2. This is consistent with the World Radiation Center (WRC) solar constant.
  - β — The transmissivity of the atmosphere (averaged over all wavelengths) for the shortest path (in the direction of the zenith).
  - m(θ) — The relative optical path length, measured as a proportion relative to the zenith path length (see equation 8 below).
  - $SunDur_{\theta,\alpha}$ — The time duration represented by the sky sector. For most sectors, it is equal to the day interval (for example, a month) multiplied by the hour interval (for example, a half hour). For partial sectors (near the horizon), the duration is calculated using spherical geometry.
  - $SunGap_{\theta,\alpha}$ — The gap fraction for the sun map sector.
  - $AngIn_{\theta,\alpha}$ — The angle of incidence between the centroid of the sky sector and the axis normal to the surface (see equation 9 below).

Relative optical length, m(θ), is determined by the solar zenith angle and elevation above sea level. For zenith angles less than 80°, it can be calculated using the following equation:

$m(\theta) = EXP(-0.000118 * Elev - 1.638*10^{-9} * Elev^2) / \cos(\theta)$ (8)

- where:
  - θ — The solar zenith angle.
  - Elev — The elevation above sea level in meters.

The effect of surface orientation is taken into account by multiplying by the cosine of the angle of incidence. Angle of incidence ($AngInSky_{\theta,\alpha}$) between the intercepting surface and a given sky sector with a centroid at zenith angle and azimuth angle is calculated using the following equation:

$AngIn_{\theta,\alpha} = acos(Cos(\theta) * Cos(G_z) + Sin(\theta) * Sin(G_z) * Cos(\alpha-G_a))$ (9)

- where:
  - G_z — The surface zenith angle.

Note that for zenith angles greater than 80°, refraction is important.

- G_a — The surface azimuth angle.

Diffuse radiation calculation

For each sky sector, the diffuse radiation at its centroid (Dif) is calculated, integrated over the time interval, and corrected by the gap fraction and angle of incidence using the following equation:

$Dif_{\theta,\alpha} = R_{glb} * P_{dif} * Dur * SkyGap_{\theta,\alpha} * Weight_{\theta,\alpha} * \cos(AngIn_{\theta,\alpha})$ (10)

- where:
  - R_{glb} — The global normal radiation (see equation 11 below).
  - P_{dif} — The proportion of global normal radiation flux that is diffused. Typically it is approximately 0.2 for very clear sky conditions and 0.7 for very cloudy sky conditions.
  - Dur — The time interval for analysis.

- $SkyGap_{\theta,\alpha}$ — The gap fraction (proportion of visible sky) for the sky sector.
- $Weight_{\theta,\alpha}$ — The proportion of diffuse radiation originating in a given sky sector relative to all sectors (see equations 12 and 13 below).
- $AngIn_{\theta,\alpha}$ — The angle of incidence between the centroid of the sky sector and the intercepting surface.

The global normal radiation (R_{glb}) can be calculated by summing the direct radiation from every sector (including obstructed sectors) without correction for angle of incidence, then correcting for proportion of direct radiation, which equals

$1\text{-}P_{dif}$:

$R_{glb} = (S_{Const}\Sigma(\beta^{m(\theta)})) / (1 - P_{dif})$ (11)

For the uniform sky diffuse model, $Weight_{\theta,\alpha}$ is calculated as follows:

$Weight_{\theta,\alpha} = (\cos\theta_2 - \cos\theta_1) / Div_{azi}$(12)

- where:
- θ_1 and θ_2 — The bounding zenith angles of the sky sector.
- Div_{azi} — The number of azimuthal divisions in the sky map.

For the standard overcast sky model, $Weight_{\theta,\alpha}$ is calculated as follows:

$Weight_{\theta,\alpha} = (2\cos\theta_2 + \cos2\theta_2 - 2\cos\theta_1 - \cos2\theta_1) / 4 * Div_{azi}$ (13)

Total diffuse solar radiation for the location (Dif_{tot}) is calculated as the sum of the diffuse solar radiation (Dif) from all the sky map sectors:

$Dif_{tot} = \Sigma\, Dif_{\theta,\alpha}$(14)

Built-Up Index Calculation

Equation 11 was used to extract the concentration of the urban built-ups from a Landsat imagery.

$$Bi = \frac{IR-NIR}{IR+NIR}$$(15)

Where;

Bi= Built-up Index

IR= Infrared

NIR= Near-Infrared

Normalized Difference Vegetation Index (NDVI)

The NDVI is based on the fact that healthy vegetation has a low reflectance in the visible portion of the electromagnetic spectrum due to chlorophyll absorption and other pigments, and high reflectance in the Near Infrared (NIR) because of the internal reflectance by the mesophyll spongy tissue of a green leaf (Campbell .J, 1987). NDVI can be calculated using pixel's reflectance values of red (visible) band and the NIR band of a satellite sensor, and is represented by the following equation 12:

$$NDVI=\frac{NIR-R}{NIR+R}$$

(16)

NDVI values range from –1 to +1. Because of the high reflectance in the NIR portion of the electromagnetic spectrum, healthy vegetation is represented by high NDVI values between 0.05 and 1. Conversely, non-vegetated surfaces (such as water bodies) yield a negative NDVI value. Bare soil areas have NDVI values which are closest to 0 due to the high reflectance in both the visible and NIR portions of the electromagnetic spectrum (Lillesand and Kiefer, 1994).

Results and Discussion

Solar Radiation

The annual Global Solar Radiation analysis generated a map (Fig 2) showing all the incoming radiation both direct and diffused. The output was calculated in the units of watt hours per square meter (WH/m^2). The high incoming radiation values which ranges from 140118 to 148731(WH/m^2) were recorded on areas 100-285m above sea level (Fig 3) such as Mbaukwu-Umuawulu axis, Nsugbe-Nkwelle-Ogbunike

axis and Nimo-EnugwuUkwu-Agukwunri- AdaziNnukwu-Agulu axis.

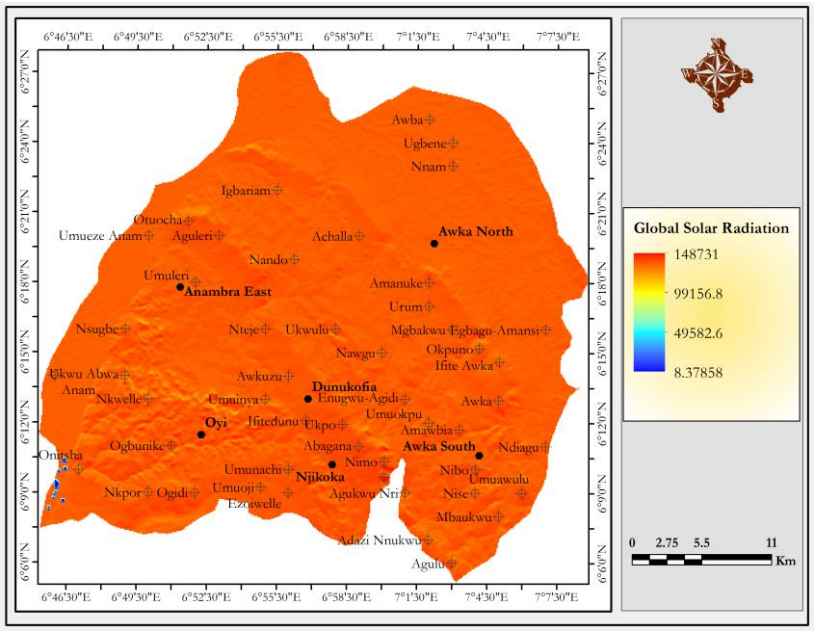


Fig 2: Global incoming solar radiation (WH/m^2)

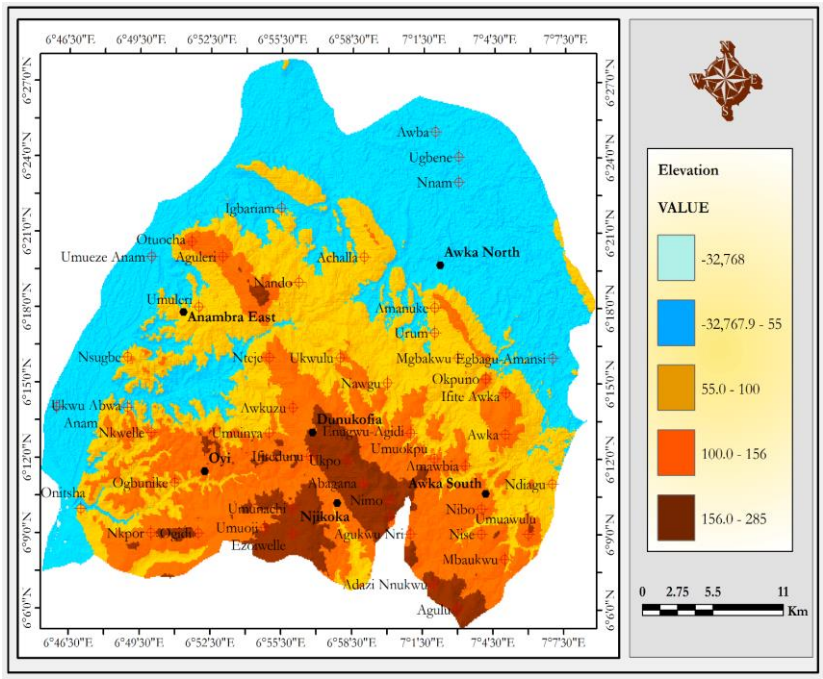


Fig 3: Elevation (m)

The annual diffused incoming solar radiation which was calculated for a standard overcast sky (Fig. 4) with units in WH/m^2. From the result, it was noted that areas with elevation value tends to diffuse the incoming solar radiation more than the lowlands. The high lands around Mbaukwu-Umuawulu axis, Nsugbe-Nkwelle-Ogbunike axis and Nimo-EnugwuUkwu-Agukwunri-AdaziNnukwu-Agulu axis has the highest found value of 35799WH/m^2 of the diffused incoming solar radiation.

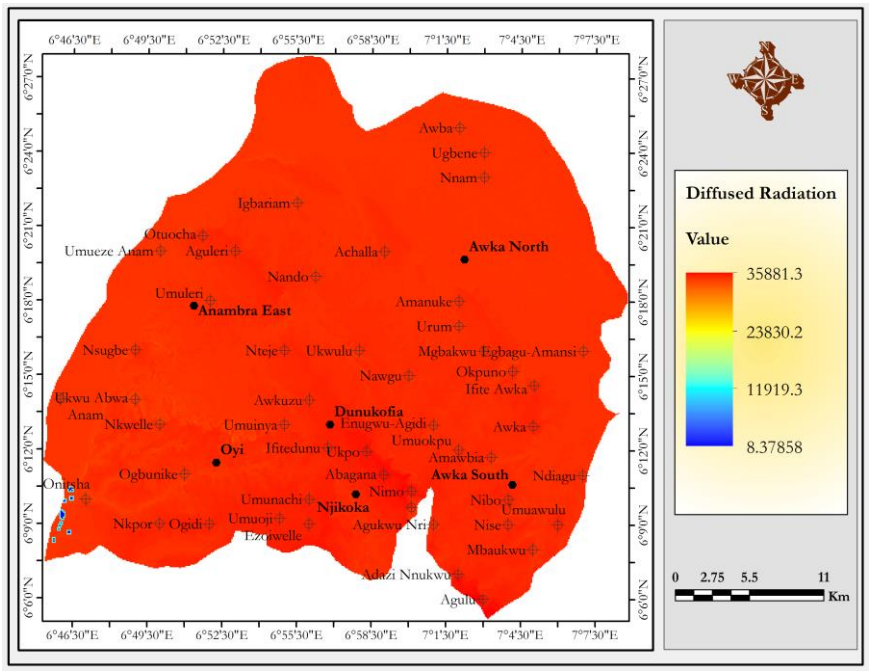


Fig 4: Diffused incoming solar radiation (WH/m^2)

The total annual direct incoming solar radiation which was calculated for a standard overcast sky (Fig5) with units in WH/m^2. From the result, it was noted that on an approximate that 90% of the study area receives a good amount of the direct incoming solar radiation.

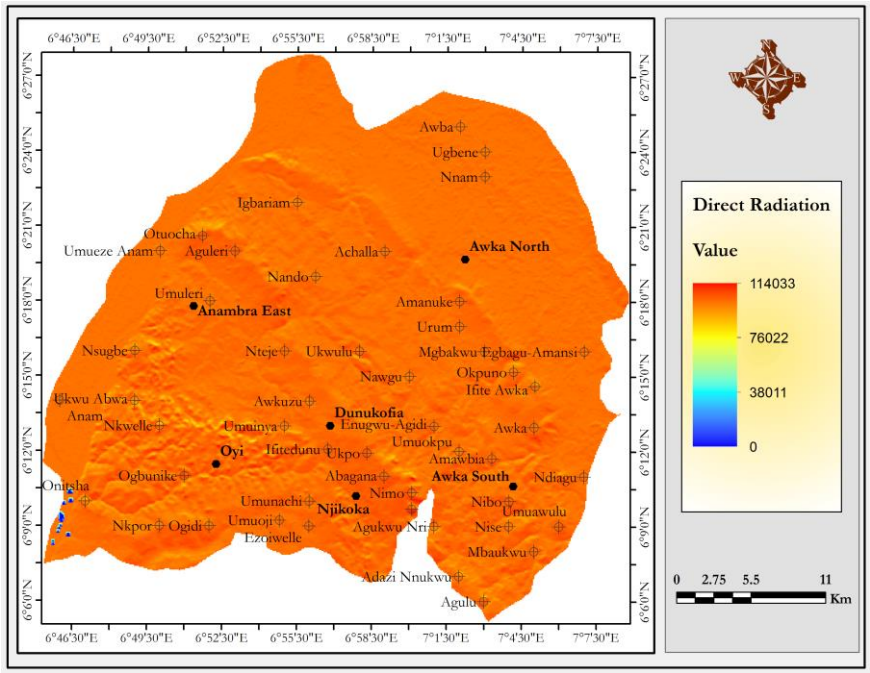


Fig5: Direct incoming solar radiation (WH/m^2)

The total annualduration of direct incoming solar radiationwas calculated in hours (Fig.6). The result shows that a large percenatge of the study area experiences a longer duration of the solar radiation with high values ranging from 350 – 356hours.

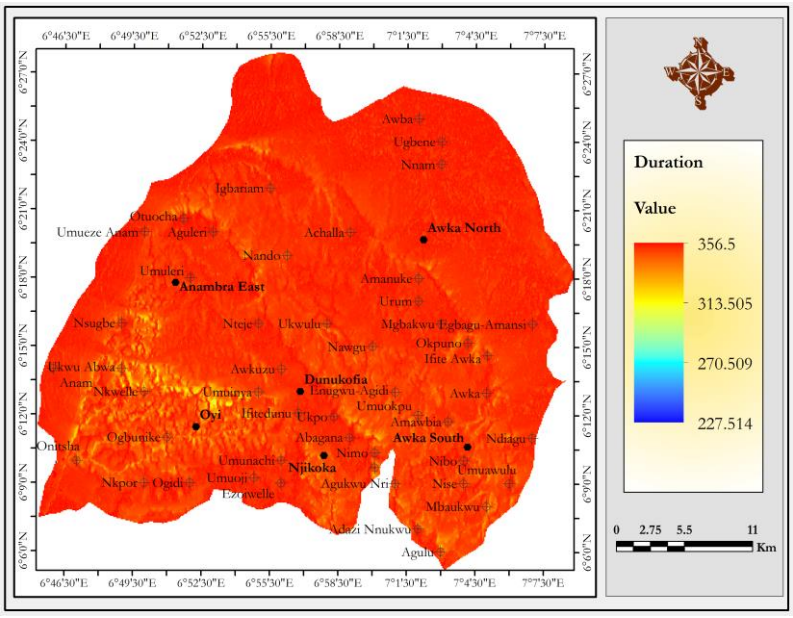


Fig 6: Duration of the incoming solar radiation (hours)

The Urban-Rural Meteorology

The Urban Heat Island results (Fig 7) as calculated shows that towns within Awka North and some parts of Awka South experiences a relatively high temperature within the range of 30-38°C more than other towns.When the results was compared to other contributing factors to UHI within the study area, from Fig 8(a) it could be seen that areas with the high temperature value are relatively covered with artificial surfaces with low vegetation cover (Fig 8b) and moderate high monthly mean rainfall (Fig 8c).

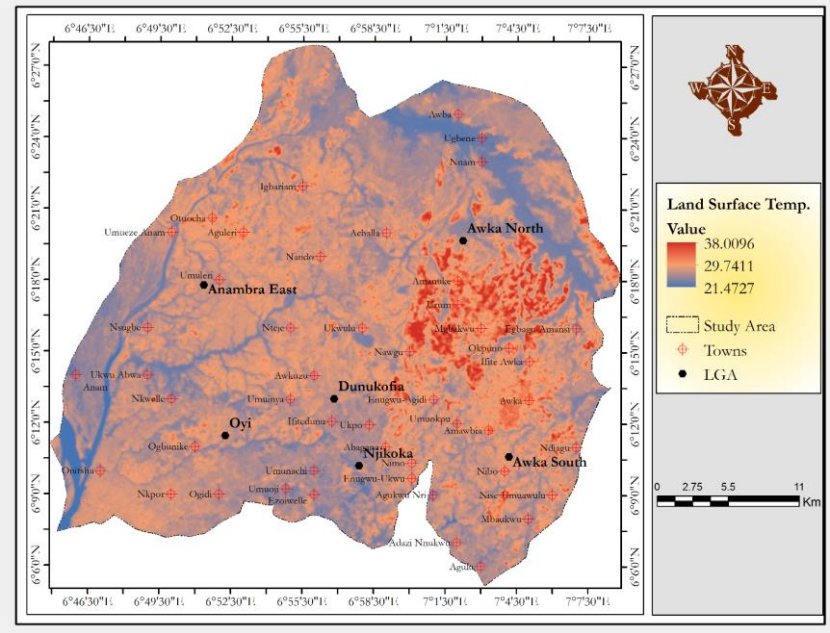


Fig 7: Land Surface Temperature

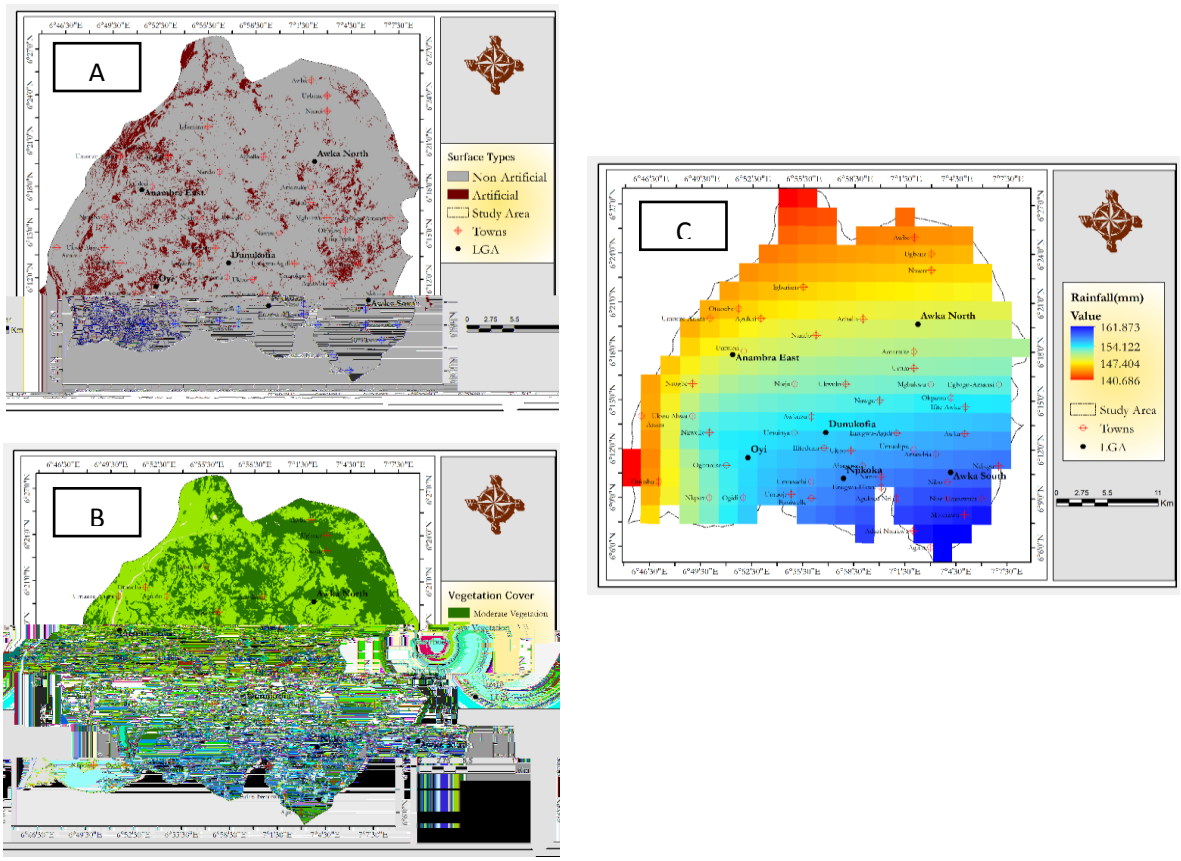


Fig8: (a) Surface Types (b) Vegetation Cover (c) Rainfall (mm)

The UHI profile illustrated in Fig 9, shows the pattern and trend of the surface temperature above the different surface types in the study area. The urban areas within the Awka city has the highest temperature value more than the rural and semi-urban areas. The temperature of the waterbody around Amansea has a relative good cooling effect on its surrounding. The moderately vegetated cover around Igbariam-Awkuzu-Nawfia-Umuokpu helped in modifying the micro-climate of the area.Nkwelle-Ogbunike area falls under the semi-urban classification zone, thus the temperature is moderately normal for human comfort.

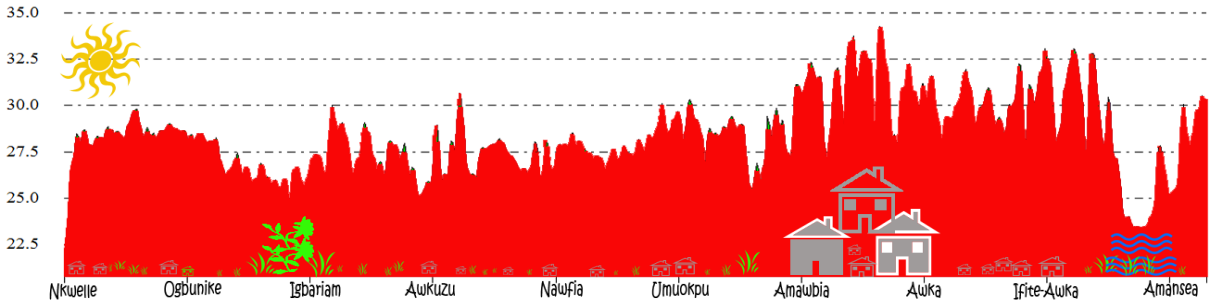


Fig9: UHI Profile

Conclusion

Topography plays an important role in determining the amount of the incoming solar radiation both direct and diffused together with the duration within a geographical area. Being that the solar radiation controls the above surface temperature, surface types (artificial and non-artificial) determines the surface temperature of an area and both controls the UHI over the geographical area.

References

Ahmed, B., Kamruzzaman, M., Zhu, X., & Rahman, M. S. (2013). Simulating Land Cover Changes and Their Impacts on Land Surface Temperature in Dhaka, Bangladesh. *Remote Sensing 5*, 5969-5998.

Asmat, A., Mansor, S., & Hong, W. (2003). Rule Based Classification for Urban Heat Island Mapping. *2nd FIG Regional Conference: TS18 GIS Tools for Application*, 1-11.

Campbell, J. (1987). *Introduction to Remote Sensing.* New York: The Guilford Press.

El-Sayed, E. O. (2012). Detection of Land-Use and Surface Temperature Change at Different Resolutions. *Journal of Geographic Information System, 4*, 189-203.

Enjun, M., Xiangzheng, D., Zhang, Q., & Liu, A. (2014). Spatial Variation of Surface Energy Fluxes Due to Land Use Changes across China. *energies 7, doi:10.3390/en7042194*, 2194-2206.

ESRI. (2014). *ArcGIS Help: Understanding solar radiation analysis.* USA: ESRI Inc.

Fu, P., & Rich, P. M. (2000). *The Solar Analyst 1.0 Manual.* USA: Helios Environmental Modeling Institute (HEMI).

Fu, P., & Rich, P. M. (2002). A Geometric Solar Radiation Model with Applications in Agriculture and Forestry. *Computers and Electronics in Agriculture 37*, 25–35.

Hara, Y., Takeuchi, K., & Okubo, S. (2005). Urbanization linked with past agricultural land use patterns in the urban fringe of a deltaic Asian mega-city: a case study in Bangkok. *Landscape Ecology and Planning, vol. 73*, 16-28.

Howard, L. (1833). The climate of London. *London Harvey Dorton, 2* , 181-1820.

Lillesand, T. M., & Kiefer, R. W. (1994). *Remote Sensing and Image Interpretation.* New York: John Wiley & Sons .

Liu, L., & Zhang, Y. (2011). Urban heat island analysis using the Landsat TM data and ASTER data: A Case study in Hong Kong. . *Remote Sens. 3*, 1535-1552.

Ohashi, Y., & Kida, H. (2002). Local circulations developed in the vicinity of both coastal and inland urban areas: A numerical study with a mesoscale atmospheric model. *J. Appl. Meteor. 41*, 30-45.

Rich, P. M., Dubayah, R., Hetrick, W. A., & Saving, S. C. (1994). Using Viewshed Models to Calculate Intercepted Solar Radiation: Applications in Ecology. *American Society for Photogrammetry and Remote Sensing Technical Papers*, 524–529.

Souch, C., & Grimmond, S. (2006). Applied climatology: Urban climate. . *Prog. Phys. Geogr. 30*, 270-279.

Streutker, D. (2002). A remote sensing study of the urban heat island of Houston, Texas. . *Int. J. Remote Sens, 23*, 2595-2608.

Tao, Z., Santanello, J., Chin, M., Zhou, S., Tan, Q., Kemp, E., & Peters-Lidard, C. (2013). Effect of land cover on atmospheric processes and air quality over the continental United States—A NASA Unified WRF (NU-WRF) model study. . *Atmos. Chem. Phys. 13*, 6207-6226.

Voogt, J. (2011). *How Researchers Measure Urban Heat Islands.* London ON Canada: Department of Geography, University of Western Ontario.

Voogt, J. A., & Oke, T. R. (2003). .Thermal remote sensing of urban climate.Remote Sensing of .

Wubet, M. T. (2003). *Estimation of Absolute Surface Temperature by Satellite Remote Sensing,.* Netherlands: M.Sc Thesis, International Institute for Geoinformation Science and Earth Observation.